Cyanide-Bridged Fe–Fe and Fe–Co Molecular Squares: Structures and Electrochemistry of $[Fe^{II}_4(\mu\text{-}CN)_4(bpy)_8](PF_6)_4\cdot 4H_2O$, $[Fe^{II}_2Co^{II}_2(\mu\text{-}CN)_4(bpy)_8](PF_6)_4\cdot 3CHCl_3\cdot 2CH_3CN$, and $[Fe^{II}_2Co^{III}_2(\mu\text{-}CN)_4(bpy)_8](PF_6)_6\cdot 2CHCl_3\cdot 4CH_3NO_2$

Hiroki Oshio,* Hironori Onodera, Osamu Tamada, Hideto Mizutani, Takashi Hikichi, and Tasuku Ito[a]

Abstract: Cyanide-bridged iron–iron and iron–cobalt molecular squares of $[Fe^{II}_4(\mu\text{-}CN)_4(bpy)_8](PF_6)_4\cdot 4H_2O$ (**1**), $[Fe^{II}_2Co^{II}_2(\mu\text{-}CN)_4(bpy)_8](PF_6)_4\cdot 3CHCl_3\cdot 2CH_3CN$ (**2**), and $[Fe^{II}_2Co^{III}_2(\mu\text{-}CN)_4(bpy)_8](PF_6)_6\cdot 2CHCl_3\cdot 4CH_3NO_2$ (**3**) (bpy = 2,2′-bipyridine) were prepared. X-ray structure analyses for **1**–**3** were performed and their electrochemistry was studied. In **1**–**3**, four metal ions are bridged by cyanide groups to form tetranuclear macrocycles ("molecular squares"). Each metal ion in the square is six-coordinate; four of the coordination sites are occupied by the nitrogen atoms of two of bpy ligands and the remaining *cis* coordination sites are occupied by cyanide-carbon or cyanide-nitrogen atoms. In **1**, Fe–C (cyanide) (1.899(4)–1.927(4) Å) and Fe–N(cyanide) (1.929(4)–1.950(4) Å) distances are typical of low-spin Fe^{2+} ions. In **2**, Fe–C(cyanide) and Co^{2+}–N(cyanide) bond lengths are in the range 1.919(5)–1.963(5) Å and 1.850(5)–2.017(5) Å, respectively; in contrast, shorter bond lengths are observed for the metal to cyanide-carbon and cyanide-nitrogen (1.878(7)–1.893(7) Å) in **3**. As a result, the molecular squares in **1**, **2**, and **3** have sides of 4.947(1)–4.986(1) Å, 5.001(1)–5.053(1) Å, and 4.910(1)–4.918(1) Å, respectively. Magnetic susceptibility measurements revealed that the Fe^{2+} and Co^{3+} ions in **1** and **3** are diamagnetic, while the high-spin Co^{2+} ions in **2** are weakly coupled through the low-spin Fe^{2+} ions. Cyclic voltammograms of the squares are presented, and the electrochemically generated mixed-valent species $[Fe^{II}_2Fe^{III}_2(\mu\text{-}CN)_4(bpy)_8]^{6+}$ was discussed in terms of the intervalence transfer band.

Keywords: cobalt · electrochemistry · iron · mixed-valent compounds · molecular squares

Introduction

Cyanide ions bridge a variety of metal ions and form assembled systems. Prussian blue analogues, cyanide-bridged infinite three-dimensional (3D) systems, have attracted intense research interest in view of their magnetic and magneto-optical properties. A variety of cyanide-bridged infinite systems formulated as $M_x[M(CN)_6]$ or $M_x[M(CN)_7]$ (M and M′ are transition metal ions) display bulk magnetism and their Curie temperature ranges from 5 K to room temperature,[1] where Prussian blue, $Fe^{III}_4[Fe^{II}(CN)_6]_3\cdot 15H_2O$, shows ferromagnetic ordering at 5.6 K.[2] External influences such as light and electrical potential have been reported to control the magnetic transition in the cyanide-bridged compounds.[3] Magnetic ordering phenomena in $Co_x[Fe(CN)_6]^{n-}$ is governed by irradiation with light; this induced electron transfers back and forth from Fe^{II} to Co^{III} and from Co^{II} to Fe^{III} sites. In contrast, hexacyanometalates $[M(CN)_6]^{n+}$ have been used to construct molecular architectures with high-spin ground states.[4] $[Cr^{III}(CN)_6]^{3-}$ ions react with metal ions or cationic complexes to give, for example, μ-cyano heptanuclear complexes with $Cr^{III}Mn^{II}_6$ and $Cr^{III}Ni^{II}_6$ cores, which have been reported to have $S = 27/2$ and 15/2 spin ground states, respectively.[5] Such high-spin molecules are expected to display new physical phenomena of spin quantum tunneling, large magnetic anisotropy, and superparamagnetism. Recently, an organometallic approach has provided a rational route to cyanide-bridged molecular boxes with Rh_8, Cr_4Co_4, and Co_8 cores.[6] The development of versatile synthetic routes to prepare mixed-metal clusters provides an opportunity to study interactions between metal ions, and structural information may help to understand the dynamic behavior in the amorphous systems. We have now synthesized a class of cyanide-bridged cluster molecules of the general formula $[Fe_2M_2(\mu\text{-}CN)_4(bpy)_6]^{n+}$ (M = the late first-row transition metal ions; bpy = 2,2′-bipyridine) in which cyanide ions bridge

[a] Prof. H. Oshio, H. Onodera, O. Tamada, H. Mizutani, Takashi Hikichi, Prof. Tasuku Ito
Department of Chemistry, Graduate School of Science
Tohoku University, Aoba-ku, Sendai 980–8578 (Japan)
Fax: (+81) 22-217-6548
E-mail: oshio@agnus.chem.tohoku.ac.jp

  0947-6539/00/0614-2523 $ 17.50+.50/0

four metal ions to form a macrocyclic tetranuclear core—a so-called molecular square. Herein we present syntheses, crystal structures, and electrochemistry of $[Fe^{II}_4(\mu\text{-}CN)_4(bpy)_8](PF_6)_4\cdot 4H_2O$ (**1**), $[Fe^{II}_2Co^{II}_2(\mu\text{-}CN)_4(bpy)_8](PF_6)_4\cdot 3CHCl_3\cdot 2CH_3CN$ (**2**), and $[Fe^{II}_2Co^{III}_2(\mu\text{-}CN)_4(bpy)_8](PF_6)_6\cdot 2CHCl_3\cdot 4CH_3NO_2$ (**3**).

Results and Discussion

Description of the structure

ORTEP diagrams of complex cations in **1**–**3** are depicted in Figure 1 and 2, and their selected bond lengths and angles are listed in Table 1.

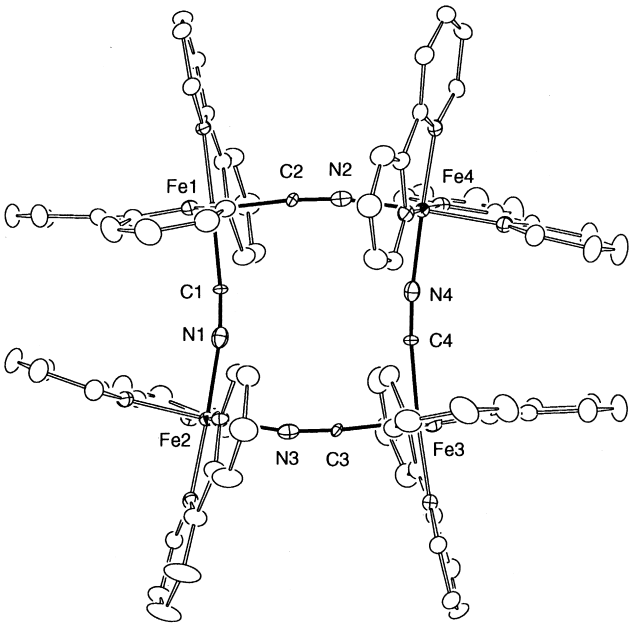

1

Figure 1. Structure of a square cation in **1** (ORTEP diagrams; 30 % probability).

Abstract in Japanese:

シアン化物イオン架橋環状４核錯体 $[Fe^{II}_4(\mu\text{-}CN)_4(bpy)_8](PF_6)_4\cdot 4H_2O$ (**1**), $[Fe^{II}_2Co^{II}_2(\mu\text{-}CN)_4(bpy)_8](PF_6)_4\cdot 3CHCl_3\cdot 2CH_3CN$ (**2**), $[Fe^{II}_2Co^{III}_2(\mu\text{-}CN)_4(bpy)_8](PF_6)_6\cdot 2CHCl_3\cdot 4CH_3NO_2$ (**3**) (bpy = 2,2'-bipyridine) を合成し，それらの構造を決定するとともにサイクリックボルタンメトリー (CV) により酸化還元挙動を調べた．化合物 **1**–**3** において４つの金属イオンはシアン化物イオンにより架橋され，一辺がそれぞれ4.947(1) – 4.986(1) Å, 5.001(1) – 5.053(1) Å, 4.910(1) – 4.918(1) Å の長さをもつ四角形の骨格構造をつくる．化合物 **1** のCVはアセトニトリル中 0.67 V と0.86 V (vs. SSCE) にシアン化物イオンの窒素原子が配位した鉄イオン(Fe^{II}/Fe^{III}) の準可逆な２段階１電子酸化還元波を示し，その２電子電解酸化体は 1380 nm (ε = 8600 $M^{-1}cm^{-1}$) に IVCT (intervalence charge transfer) 吸収帯をもつクラス II の混合原子価錯体である．Hushのモデルに基づく解析により H_{AB} (resonance energy) および α^2 (electronic delocalization) がそれぞれ 870 cm^{-1}，0.014と見積もられた．化合物 **3** のCV は 0.23 V～0.47 V にコバルトイオン (Co^{II}/Co^{III}) の１段階２電子酸化還元波，1.38 Vと1.51 Vに鉄イオン (Fe^{II}/Fe^{III}) の２段階１電子酸化還元波を示した．一方，化合物 **2** は複雑な酸化還元過程を示し，これは酸化還元に伴う４核骨格の構造変化により説明された．

Table 1. Bond lengths [Å] and angles [°] of core structures in **1**–**3**.

$[Fe^{II}_4(\mu\text{-}CN)_4(bpy)_8](PF_6)_4\cdot 4H_2O$ (**1**)			
Fe(1)–C(1)	1.899(4)	Fe(1)–C(2)	1.915(4)
Fe(2)–N(1)	1.932(5)	Fe(2)–N(3)	1.950(4)
Fe(3)–C(4)	1.905(4)	Fe(3)–C(3)	1.927(4)
Fe(4)–N(4)	1.929(4)	Fe(4)–N(2)	1.939(4)
N(1)–C(1)	1.149(6)	N(2)–C(2)	1.154(6)
N(3)–C(3)	1.144(6)	N(4)–C(4)	1.153(6)
Fe(1)···Fe(2)	4.963(1)	Fe(2)···Fe(3)	4.986(1)
Fe(3)···Fe(4)	4.947(1)	Fe(1)···Fe(4)	4.975(1)
Fe(1)···Fe(3)	7.009(2)	Fe(2)..Fe(4)	6.927(1)
C(1)-Fe(1)-C(2)	89.9(2)	N(1)-Fe(2)-N(3)	88.9(2)
C(4)-Fe(3)-C(3)	90.5(2)	N(4)-Fe(4)-N(2)	89.7(2)
C(1)-N(1)-Fe(2)	170.7(4)	C(2)-N(2)-Fe(4)	170.5(4)
C(3)-N(3)-Fe(2)	169.0(4)	C(4)-N(4)-Fe(4)	173.9(4)
N(1)-C(1)-Fe(1)	172.3(4)	N(2)-C(2)-Fe(1)	173.5(4)
N(3)-C(3)-Fe(3)	175.4(4)	N(4)-C(4)-Fe(3)	173.2(4)
$[Fe^{II}_2Co^{II}_2(\mu\text{-}CN)_4(bpy)_8](PF_6)_4\cdot 3CHCl_3\cdot 2CH_3CN$ (**2**)			
Fe(1)–C(1)	1.919(5)	Fe(1)–C(4)	1.919(4)
Fe(2)–C(2)	1.952(5)	Fe(2)–C(3)	1.963(5)
Co(1)–N(2)	1.980(5)	Co(1)–N(1)	1.994(5)
Co(2)–N(4)	1.996(4)	Co(2)–N(3)	2.017(5)
N(1)–C(1)	1.142(6)	N(2)–C(2)	1.135(6)
N(3)–C(3)	1.115(6)	N(4)–C(4)	1.121(6)
Fe(1)···Co(1)	5.005(1)	Fe(1)···Co(2)	5.001(1)
Fe(2)···Co(1)	5.034(1)	Fe(2)···Co(2)	5.053(1)
Fe(1)···Fe(2)	7.010(2)	Co(1)···Co(2)	7.173(1)
C(1)-Fe(1)-C(4)	91.94(17)	C(2)-Fe(2)-C(3)	91.73(19)
N(2)-Co(1)-N(1)	91.17(17)	N(4)-Co(2)-N(3)	89.86(17)
C(1)-N(1)-Co(1)	166.7(4)	C(2)-N(2)-Co(1)	170.2(4)
C(3)-N(3)-Co(2)	167.9(4)	C(4)-N(4)-Co(2)	172.5(4)
N(1)-C(1)-Fe(1)	174.8(4)	N(2)-C(2)-Fe(2)	174.4(4)
N(3)-C(3)-Fe(2)	173.6(5)	N(4)-C(4)-Fe(1)	171.8(4)
$[Fe^{II}_2Co^{III}_2(\mu\text{-}CN)_4(bpy)_8](PF_6)_6\cdot 2CHCl_3\cdot 4CH_3NO_2$ (**3**)			
Co–N(1)	1.893(6)	Co–N(2)	1.887(6)
Fe–C(1)	1.878(7)	Fe–C(2)	1.893(7)
N(1)–C(1)	1.151(8)	N(2)–C(2)*	1.161(8)
Fe···Co	4.918(1)	Fe···Co*	4.910(1)
Fe···Fe*	6.983(2)	Co···Co*	6.916(1)
N(2)-Co-N(1)	89.9(2)	C(1)-Fe-C(2)	88.9(3)
C(1)-N(1)-Co	175.6(6)	C(2)*-N(2)-Co	171.9(6)
N(1)-C(1)-Fe	175.5(6)	N(2)*-C(2)-Fe	173.4(6)

Key to symmetry operation: * $-x+1, -y+1, -z+1$.

$[Fe^{II}_4(\mu\text{-}CN)_4(bpy)_8](PF_6)_4\cdot 4H_2O$ (1): Complex cation **1** is a tetranuclear macrocycle composed of four cyanide-bridged low-spin Fe^{2+} ions, and the overall geometry of the macrocycle is nearly square (Figure 1). The iron ions in the square are six-coordinate; four coordination sites are occupied by four nitrogen atoms from two bpy ligands and the remaining *cis* positions are coordinated by either carbon or nitrogen atoms of the cyanide groups. In the cyanide ions, the carbon and nitrogen atoms act as π acceptor and σ donor, respectively, and this Lewis acid–base character increases the π-bonding and σ-antibonding character of the iron ion with the cyanide-carbon and -nitrogen atoms.[7] Therefore, it is reasonable to expect that the Fe^{II}–C(cyanide) bond length is shorter than the Fe^{II}–N(cyanide) bond length. The Fe^{II}–N(cyanide) and Fe^{II}–C(cyanide) distances lie in the range 1.929(4)–1.950(4) Å and 1.899(4)–1.927(4) Å, respectively, while the Fe^{II}–N(bpy) bond lengths are between 1.950(4) and 1.981(4) Å. The C-Fe^{II}-C and N-Fe^{II}-N bond angles are close to a right angle (88.9(2)–90.5(2)°); the Fe^{II}-N-C and Fe^{II}-C-N bond angles (169.0(4)–175.4(4)°), however, deviate from 180°, characteristic of the sp hybridization of the cyanide

0947-6539/00/0614-2524 $ 17.50+.50/0 *Chem. Eur. J.* **2000**, *6*, No. 14

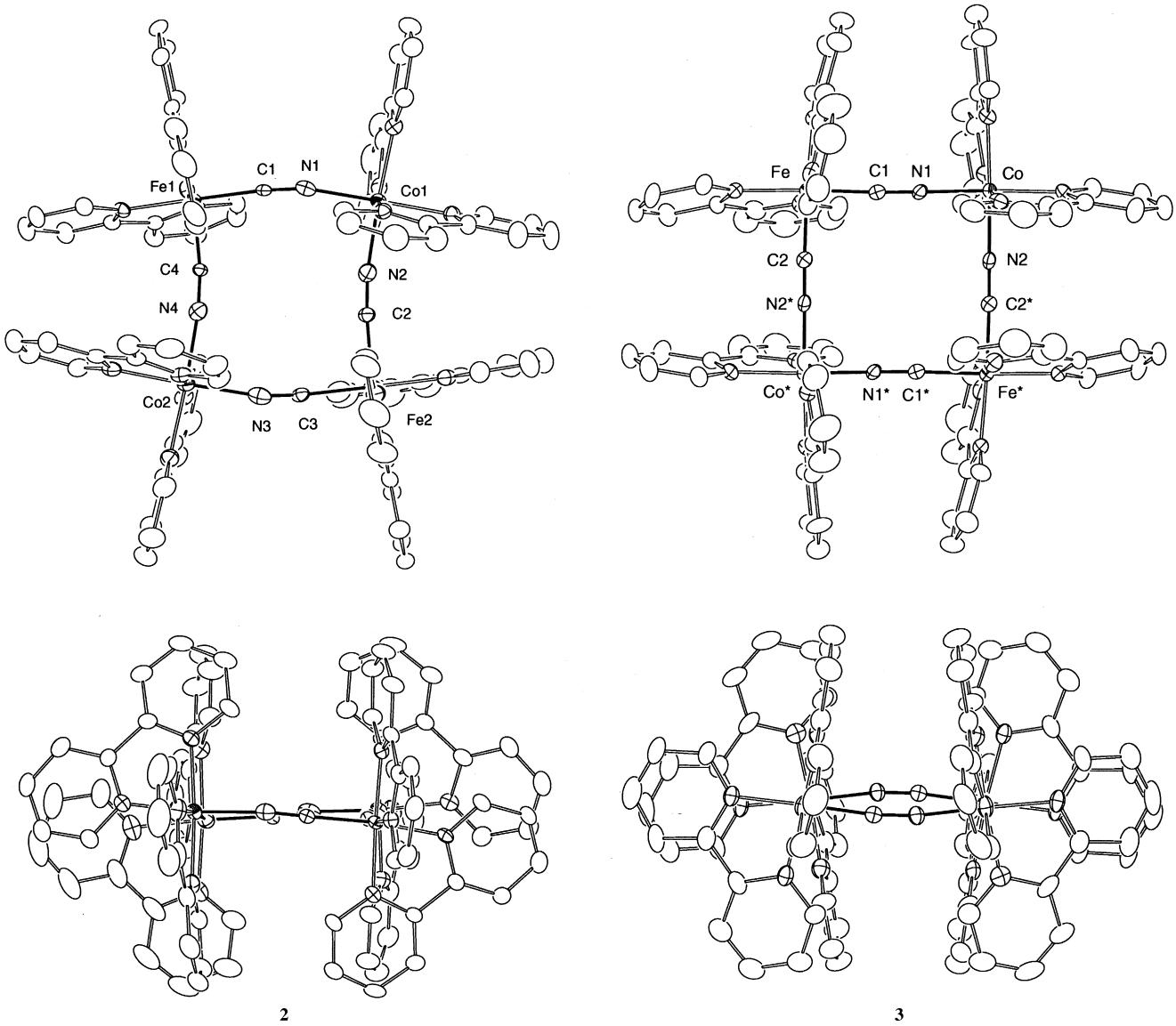

Figure 2. Structures of the of square cations in **2** and **3** (ORTEP diagrams; 30 % probability). Top: top view; bottom: side view.

group. The strong π-back donation imposes pronounced sp^2 character on the cyanide, which results in the deviation from 180°. In the square of **1**, the cyanide bridges separate the two Fe^{2+} ions with interatomic distances of 4.947(1) – 4.986(1) Å.

$[Fe^{II}_2Co^{II}_2(\mu\text{-}CN)_4(bpy)_8](PF_6)_4 \cdot 3CHCl_3 \cdot 2CH_3CN(PF_6)_4$ (2): Complex **2** crystallizes in the triclinic space group $P\bar{1}$. The square in **2** is composed of Fe^{2+} (low-spin) and Co^{2+} (high-spin) ions alternately bridged with the cyanide ions; the coordination sites of the six-coordinate metal centers are occupied by four nitrogen atoms from two bpy ligands and either two cyanide-carbon or -nitrogen atoms. In the structure analysis of **2** (Figure 2), the assignment of metal ions, cyanide-carbon and -nitrogen atoms is sometimes difficult. Taking into consideration that the π-back bonding character of a Fe^{2+} ion is stronger than that of a Co^{2+} ion, the Fe^{2+} ions should be coordinated by the cyanide-carbon atoms, and as a result the Fe^{II}–C(cyanide) bonds should be shorter than the Co^{II}–N-(cyanide) bonds. Thus, the combinations with the shorter metal-to-ligand distances were assigned to the Fe–C(cyanide) pairs. In **2**, the Fe^{II}–C and Co^{II}–N (cyanide) bond lengths are 1.919(5) – 1.963(5) Å and 1.994(5) – 2.015(5) Å, respectively, while the Fe^{II}–N(bpy) (1.978(4) – 2.039(4) Å) and Co^{2+}–N(bpy) (2.018(5) – 2.056(4) Å) bond lengths are slightly longer. The C-Fe^{II}-C and N-Co^{II}-N bond angles range between 89.86(17) and 91.94°. The square in **2** has the edge-to-edge distances ($Fe^{II} \cdots Co^{II}$) of 5.001(1) – 5.053(1) Å. Individual squares in **1** and **2** are chiral, but the crystal as a whole is racemic. Each metal ion in the squares **1** and **2** has either a $\Lambda\Lambda\Lambda\Lambda$ or a $\Delta\Delta\Delta\Delta$ configuration.

$[Fe^{II}_2Co^{III}_2(\mu\text{-}CN)_4(bpy)_8](PF_6)_6 \cdot 2CHCl_3 \cdot 4CH_3NO_2$ (3): Complex **3** crystallizes in the monoclinic space group $P2_1/n$ and the complex cation resides on a center of inversion. In **3** the tetranuclear core has the absolute configurations of either $\Lambda\Lambda\Delta\Delta$ or $\Delta\Delta\Lambda\Lambda$ for the Fe^{2+}, Co^{3+}, Fe^{2+}, and Co^{3+} ions. In **3**, six-coordinate Fe^{2+} (low-spin) and Co^{3+} (low-spin) ions are alternately bridged by the cyanide ions. Observed bond lengths between the metal and cyanide-carbon or -nitrogen atoms in **3** are quite similar, therefore, the assignments of

metal ions and cyanide carbon or nitrogen atoms are tentative and remain ambiguous. The orientation of the cyanide groups might be disordered. The bond lengths between the metal ions and cyanide-carbon or cyanide-nitrogen atoms are the shortest for the squares reported herein (1.878(7) – 1.893(7) Å). The C–N(cyanide) distances (1.151(8) and 1.161(8) Å) in **3** are longer than those observed in **1** (1.144(6) – 1.154(6) Å) and **2** (1.115(6) – 1.142(6) Å). In **3**, the π-back donation leading to the long C–N(cyanide) and short Fe^{2+}–C bond lengths is more pronounced since the Co^{3+} moieties can act as Lewis acids. The sides of the square ($Fe^{2+}\cdots Co^{3+}$) are 4.910(1) and 4.918(1) Å and in this case the angular deviation from a right angle is less than 2°.

Magnetic properties and IR spectra

Magnetic susceptibility measurements reveal that **1** and **3** are diamagnetic, which implies the Fe^{2+} and Co^{3+} ions are in the low-spin state. In **2**, the high-spin Co^{2+} ions are antiferromagnetically coupled through the diamagnetic Fe^{2+} ions and the exchange coupling constant $J(H=-2JS_{Co}S_{Co})$ was estimated to be $-2.7\ cm^{-1}$.

CN stretching frequencies of the cyanide groups are generally sensitive to the bond lengths (d_{C-N}) of the CN groups and to the oxidation state of the coordinated metal ions. The C–N bond lengths in $[Fe(CN)_2(phen)_2]$[8] and $[Fe(CN)_2(bpy)_2](ClO_4)$[9] are 1.149(7) – 1.151(7) Å and 1.123(9) – 1.135(1) Å, respectively, and the former showed strong IR signals of ν(CN) at 2075 and 2062 cm^{-1}, whereas the latter has a barely detectable IR band at 2120 cm^{-1}.[9] Table 2 lists the ν(CN) frequencies of the cyanide groups in **1** – **3**.

Table 2. ν(CN) stretching frequencies in **1** – **3** and related compound.

Compound	ν(CN)/cm^{-1}
$[Fe^{II}(CN)_2(bpy)_2]$	2074
1	2083, 2112, 2129
2	2095
3	2125

X-ray structure analyses showed that the CN bond lengths in **1** – **3** (d_{C-N} = 1.144(6) – 1.154(6) (**1**), 1.115(6) – 1.142(6) (**2**), and 1.151(8) – 1.161(8) Å (**3**)) depend on the metal ions and their oxidation states. However, the ν(CN) frequencies in the square do not show systematic changes with the C–N bond lengths.

Electrochemistry

Cyclic voltammograms of **1** – **3** were measured in CH_3CN containing of 0.1 M $[(tBu)_4N](PF_6)$ at a scan rate of 100 mV s^{-1} at 20 °C. The cyclic voltammetric data for **1** – **3** are summarized in Table 3.

$[Fe^{II}_4(\mu\text{-}CN)_4(bpy)_8](PF_6)_4\cdot 4H_2O$ (1): The square cations in **1** are abbreviated as $[Fe(CN)Fe(NC)Fe(CN)Fe(NC)]^{n+}$. The cyclic voltammogram (Figure 3) of **1** showed quasi-reversible waves at 0.67 V (ΔE_p = 70 mV) and 0.86 V (ΔE_p = 80 mV) versus SSCE, followed by an irreversible wave at 1.37 V.[10]

Table 3. Cyclic voltammetry data V versus SSCE for **1** – **3**.

Compound	E_{pa}[a]	E_{pc}[a]	$E_{1/2}$[b]
$[Fe^{II}(CN)_2(bpy)_2]$	0.51	0.43	0.47
1	0.70	0.63	0.67
	0.90	0.82	0.86
2	0.9	0.23	
	1.1		
	1.51	1.39	1.45
3	0.47	0.23	–
	1.42	1.34	1.38
	1.55	1.47	1.51

[a] Volts vs SSCE, a glassy carbon working electrode, CH_3CN containing 0.1 M $[tBu_4N]PF_6$, scan rate of 100 mV s^{-1}, 20 °C. [b] $E_{1/2}=(E_{pa}+E_{pc})/2$.

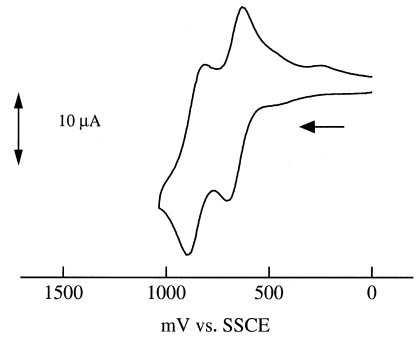

Figure 3. Cyclic voltammogram of **1** in acetonitrile.

Controlled potential coulometry at 1.0 V revealed that the two quasi-reversible waves correspond to an overall two-electron process. In the square of **1**, two coordination sites of the Fe^{2+} ions are occupied by either cyanide-carbon or -nitrogen atoms. The d orbitals of the Fe^{2+} ion with the cyanide-carbon atoms were stabilized by the π-back donation, while the σ-donor character of the cyanide-nitrogen destabilizes the d orbitals of the Fe^{2+} ion. Therefore, the first two quasi-reversible processes occur at the Fe^{2+} ions coordinated to the cyanide-nitrogen atoms. The first two-step redox behavior is interpreted as shown in Equation (1).

$$[Fe^{II}(CN)Fe^{II}(NC)Fe^{II}(CN)Fe^{II}(NC)]^{4+} \underset{+e}{\overset{-e}{\rightleftharpoons}} [Fe^{II}(CN)Fe^{III}(NC)Fe^{II}(CN)Fe^{II}(NC)]^{5+} \underset{+e}{\overset{-e}{\rightleftharpoons}} [Fe^{II}(CN)Fe^{III}(NC)Fe^{II}(CN)Fe^{III}(NC)]^{6+} \quad (1)$$

The separation between the first and second redox waves at 0.67 and 0.86 V is a measure of the stability of the mixed-valent species, $[Fe^{II}(CN)Fe^{III}(NC)Fe^{II}(CN)Fe^{II}(NC)]^{5+}$, which is imparted by the electron delocalization. This is generally represented as a comproportionation constant K_c defined as in Equation (2).

$$[Fe^{II}(CN)Fe^{II}(NC)Fe^{II}(CN)Fe^{II}(NC)]^{4+} + [Fe^{II}(CN)Fe^{III}(NC)Fe^{II}(CN)Fe^{III}(NC)]^{6+} \overset{K_c}{\rightleftharpoons} 2[Fe^{II}(CN)Fe^{III}(NC)Fe^{II}(CN)Fe^{II}(NC)]^{5+} \quad (2)$$

The observed peak separation (ΔE = 0.19 V) yields the comproportionation constant $K_c=2.4\times10^3$ in Equation (2), which indicates a moderate thermodynamic stability for the

0947-6539/00/0614-2526 $ 17.50+.50/0 *Chem. Eur. J.* **2000**, *6*, No. 14

mixed-valent species. On the other hand, the irreversible wave at 1.37 V can be assigned to the oxidation wave of the Fe^{2+} ion coordinated by the cyanide-carbon atoms. The separation between the potentials for the second and the third oxidation steps is very large (0.51 V = 1.37 – 0.86 V). The electrochemistry of polynuclear ruthenium complexes has been extensively studied;[11] a trinuclear cyanide-bridged ruthenium complex, $[NC\text{-}Ru(bpy)_2\text{-}CN\text{-}Ru(bpy)_2\text{-}NC\text{-}Ru(bpy)_2\text{-}CN](PF_6)_2$, showed cyclovoltammetric waves at 0.66 and 1.19 V (vs. SCE), which were assigned to the redox waves of cyanide-nitrogen- and -carbon-coordinated Ru^{2+} ions, respectively.[12] The observed potential separation (0.503 V) has a contribution from the asymmetry of the bridged cyanide; however, it was pointed out by Bignozzi et al.[11] that based on the analysis of MLCT bands the redox asymmetry should not contribute more than 0.2 – 0.3 V to the potential separation. In this case the degree of separation attributable to the electron delocalization through the cyanide bridges was estimated to be about 0.3 V. The observed large separation (0.51 V) for **1** can be justified on the basis of the redox asymmetry and the electron delocalization factor, which was confirmed by the observation of an intervalence transition (IT) band in the electrochemically generated $[Fe^{II}(CN)Fe^{III}(NC)Fe^{II}(CN)Fe^{III}(NC)]^{6+}$ state.

The electronic spectrum of **1** in acetonitrile was measured (Figure 4) together with controlled-potential absorption spectra performed at – 30 °C. The UV region of the spectrum of **1** is dominated by the $\pi - \pi^*$ transition of the bpy ligands, while the visible region of the spectrum of **1** consists of metal-to-ligand charge transfer (MLCT)($d - \pi^*$) transitions characteristic of the $[Fe(bpy)_2]^{2+}$ unit. As the $[Fe^{II}(CN)Fe^{III}(NC)Fe^{II}(CN)Fe^{II}(NC)]^{5+}$ state is generated for **1** on one-electron oxidation at 0.76 V (vs. SSCE), the intensity of the MLCT band at 564 nm ($\varepsilon = 20000\,M^{-1}cm^{-1}$) decreases and its maximum is blue-shifted and a new band grows in the near-IR region. After two-electron oxidation at 1.0 V, the MLCT band shifts to the higher energy region and its intensity decreases and a new band appears at 1380 nm ($\varepsilon = 8600\,M^{-1}\,cm^{-1}$), which can be assigned to the metal-to-metal intervalence transition (IT) for the $[Fe^{II}(CN)Fe^{III}(NC)Fe^{II}(CN)Fe^{III}(NC)]^{6+}$ state. When the results derived by Hush[13] for mixed-valent complexes is applied to the $[Fe^{II}(CN)Fe^{III}(NC)Fe^{II}(CN)\text{-}Fe^{III}(NC)]^{6+}$ state, the parameters of the IT band ($\varepsilon = 4300\,M^{-1}cm^{-1}$ for two chromophores, $\nu\nu_{max} = 7230\,cm^{-1}$, and $\Delta\tilde{\nu}_{1/2} = 1450\,cm^{-1}$) with the iron – iron distance (5 Å) taken from the X-ray data led to an electronic interaction matrix element (H_{AB}) of 870 cm^{-1} and a degree of electronic delocalization (α^2) of 0.014. The value of α^2 is comparable to the reported data for dinuclear ion of $[(CN)_5Fe^{III}(NC)\text{-}Fe^{II}(CN)_5]^{6-}$ ($\alpha^2 = 0.03$).[14] The small degree of delocalization, which is in contrast to larger delocalizaion in the reported dinuclear complex of $[NC\text{-}Ru(bpy)_2\text{-}(CN)\text{-}Ru(bpy)_2\text{-}CN]^{2+}$ ($H_{AB} = 2000\,cm^{-1}$ and $\alpha^2 = 0.07$),[15] shows the class II behavior.[16]

$[Fe^{II}_2Co^{II}_2(\mu\text{-}CN)_4(bpy)_8](PF_6)_4 \cdot 3CHCl_3 \cdot 2CH_3CN(PF_6)_4$ (2) and $[Fe^{II}_2Co^{III}_2(\mu\text{-}CN)_4(bpy)_8](PF_6)_6 \cdot 2CHCl_3 \cdot 4CH_3NO_2$ (3): In this section, electrochemically generated valence states of the squares in **2** and **3** are abbreviated as $[Fe^{II}_{2-n}Fe^{III}_n\text{-}Co^{II}_{2-m}Co^{III}_m]^{(4+n+m)+}$ [**2**] and [**3**] (n and $m = 0$, 1 or 2), respectively. The cyclic voltammogram of **3** in CH_3CN containing 0.1 M $[(tBu)_4N](PF_6)$ at 20 °C is shown in Figure 5.

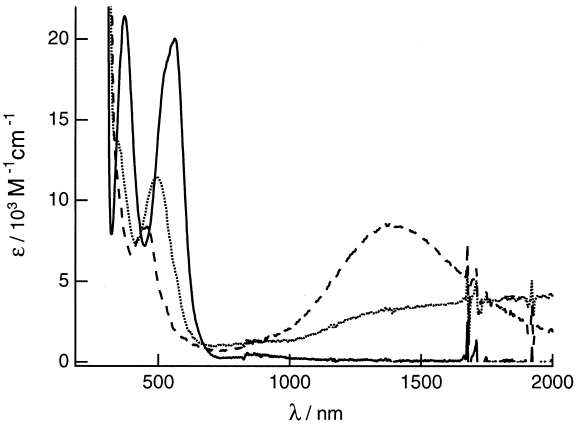

Figure 4. Electronic absorption spectra for **1** in the isolated (solid line), one-electron (dotted line), and two-electron oxidized (broken line) states. Spectroelectrochemical experiments were carried out at – 30 °C in an optical transparent thin-layer electrode made of a platinum grid placed between the window of a 2 mm spectrophotometric cell directly mounted on a spectrophotometer. Electrochemical oxidations were carried out with the counter electrode of Pt wire separated from the cathodic compartment by a frit, and Pt wire and SSCE were used for counter and reference electrodes, respectively.

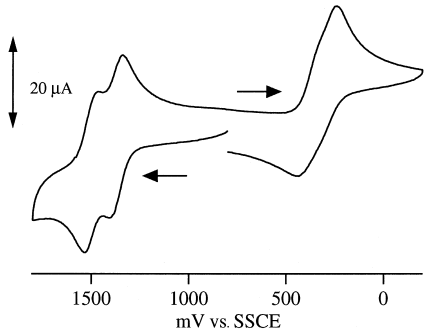

Figure 5. Cyclic voltammogram in **3** in acetonitrile.

The cyclic voltammogram of **3** shows unresolved waves at 0.23 – 0.47 V and resolved double waves at 1.38 and 1.51 V (versus SSCE), and the former redox waves can be analyzed to be superimposed double waves at 0.28 and 0.43 V by using Taube's analysis.[17] In the square of **1**, the Fe^{2+} ions coordinated to the cyanide-nitrogen atoms are oxidized at potentials of 0.67 and 0.86 V. The first two closely spaced waves at 0.28 and 0.43 V can be, therefore, assigned to the one-electron processes at cobalt centers (Co^{II}/Co^{III}), while the well-resolved double waves at 1.37 and 1.51 V correspond to the two-step one-electron transfer processes (Fe^{II}/Fe^{III}) at the iron centers coordinated by the cyanide-carbon atoms as shown in Equation (3).

$$[Fe^{III}_2Co^{III}_2]^{8+}[\mathbf{3}] \underset{-e}{\overset{+e}{\rightleftharpoons}} [Fe^{II}Fe^{III}Co^{III}_2]^{7+}[\mathbf{3}] \underset{-e}{\overset{+e}{\rightleftharpoons}} [Fe^{II}_2Co^{II}Co^{III}]^{5+}[\mathbf{3}] \underset{-e}{\overset{+e}{\rightleftharpoons}} [Fe^{II}_2Co^{II}_2]^{4+}[\mathbf{3}] \quad (3)$$

The cyclic voltammogram of **2** (Figure 6) shows quite different behavior from that of **3**. When the cyclic voltammogram was measured in the potential range from -0.2 to $+1.7$ V (vs. SSCE), three oxidation peaks at 0.9, 1.1 and 1.51 V

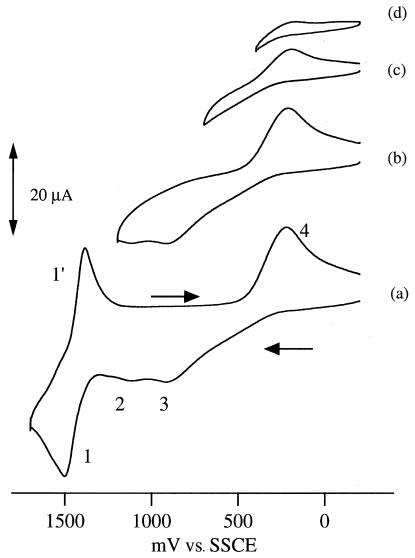

Figure 6. Cyclic voltammogram of of **2** in acetonitrile from a) -0.2 to $+1.7$ V, b) -0.2 to $+1.2$ V, c) -0.2 to $+0.7$ V, and d) -0.2 to $+0.4$ V.

(labeled 3, 2, and 1) are seen on the positive potential scan, while two reduction peaks at 1.39 and 0.23 V (labeled 1′ and 4) are observed on the subsequent negative scan. The quasi-reversible anodic wave at $E_1^{1/2} = 1.45$ V ($= (1.51+1.39)/2$) can be assigned to a two-electron process (for two Fe centers) leading to $[Fe_2^{III}Co_2^{III}]^{8+}$[**2**]. The peak 4 was not observed in the cyclic voltammogram recorded for the potential scan from -0.2 V to 0.4 V; however, the peak 4 increased as the scans were made to higher positve potentials (0.7 – 1.7 V; Figure 6a – d). Considering peak potential and current, the peaks 3 and 2 arise from the oxidation to $[Fe_2^{II}Co^{III}Co^{II}]^{5+}$[**2**] and $[Fe_2^{II}Co_2^{III}]^{6+}$[**2**], respectively, and the peak 4 is attributable to the reduction to $[Fe_2^{II}Co_2^{II}]^{4+}$[**2**]. The possible electron transfer processes are outlined in Scheme 1.

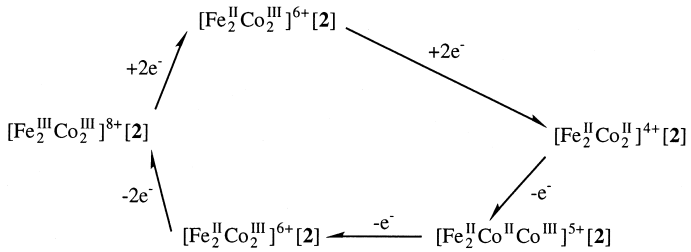

Scheme 1.

The cyclic voltammograms of **2** and **3** showed quite different electron transfer processes, which can be understood by the structures of the squares. X-ray structure analyses revealed that the distances between the metal ions and the cyanide-carbon and -nitrogen atoms in **3** (1.878(7) – 1.893(7) Å) are shorter than those in **2** (1.919(5) – 2.017(5) Å). As a result, the square in **3** (4.910(1) – 4.918(1) Å) is smaller than that in **2** (5.001(1) – 5.053(1) Å). The difference in bond lengths and size can be understood in terms of the acidity of the cobalt ions. The Co^{3+} ions in **3** act as a stronger Lewis acid than the Co^{2+} ions in **2**, which prompts the π-back donation of the Fe^{2+} ion to the cyanide groups in **3**. It can be expected that the size of the $[Fe_2^{II}Co_2^{II}]^{4+}$ cores in **2** and **3** becomes smaller as the core is oxidized. On the other hand, the ligand bpy in **2** and **3** forms intra-square $\pi-\pi$ stacks. The shortest interatomic distances (Figure 2) between the stacked bpy ligands in **3** (C15 $\cdots$ C25 3.66(1) Å) is found to be longer than that in **2** (C16 $\cdots$ C82 3.516(8) Å and C37 $\cdots$ C63 3.53(1) Å), in spite of the fact that the square in **3** is smaller than that in **2**. As $[Fe_2^{II}Co_2^{II}]^{4+}$[**2**] is electrochemically oxidized, the closer contact of the stacked bpy ligands interferes with the shrinking of the square and this might lead to the two-step oxidation with higher potential than for **3**, while $[Fe_2^{II}Co_2^{II}]^{4+}$[**3**] is not so sterically hindered as the core is oxidized. When the Co^{3+} ions in $[Fe_2^{II}Co^{II}Co^{III}]^{5+}$[**2**] $[Fe_2^{II}Co_2^{III}]^{6+}$[**2**], and $[Fe_2^{III}Co_2^{III}]^{8+}$[**2**] states are reduced to Co^{2+} ions, that is in negative potential scans, no steric hindrance exists for the expansion of the square and the cores are reduced at the same potential as in **3**. However, at present it is unclear whether the iron sites in **3** showed two-step electron transfer process in contrast to the one-step two electron transfer process in **2**, although the electronic interaction between the iron centers through the CN-Co^{3+}-NC groups are weak for both **2** and **3**.

Conclusion

$Co_x[Fe(CN)_6]$ has been proven to show photo-induced magnetic ordering, resulting from the light-induced electron transfer between Co^{2+} and Fe^{3+} or between Fe^{2+} and Co^{3+} ions.[3] We have carried out a photo-irradiation experiment on the mixed-valent square of $[Fe_2^{II}Co_2^{III}(\mu\text{-}CN)_4(bpy)_8](PF_6)_6 \cdot 2CHCl_3 \cdot 4CH_3NO_2$ (**3**) in butylonitrile solution at 7 K. We expected that a photo-induced electron-transferred species (high-spin species) of $[Fe^{II}Fe^{III}Co^{III}Co^{II}(\mu\text{-}CN)_4(bpy)_8]^{6+}$ would be observed. UV/Vis spectra of **3** before and after the light irradiation (400 nm to 700 nm by using a Xenon ramp with filters) were, however, identical, indicating that the electron transfer either did not take place or that the back electron transfer process was too rapid to be detected at this temperature.

Cyanide ions have the potential to form assemblies with metal ions and propagate not only magnetic but also electronic interactions, which are closely related. It should be possible to introduce a variety of metal ions into the molecular squares, the structural and physicochemical studies of which should allow a better understanding of metal – metal interactions mediated by cyanide bridges.

Experimental Section

Syntheses: All chemicals were used as received without further purification.

0947-6539/00/0614-2528 $ 17.50+.50/0 *Chem. Eur. J.* **2000**, *6*, No. 14

$[Fe^{II}_4(\mu\text{-}CN)_4(bpy)_8](PF_6)_4\cdot 4H_2O$ (1): All procedures were carried out under nitrogen atmosphere. A solution of $FeCl_2\cdot 4H_2O$ (0.08 mg, 0.4 mmol) in methanol (10 mL) was added to a solution of $[Fe(CN)_2(bpy)_2]$[18] (0.17 g, 0.4 mmol) in methanol (10 mL). To the resulting dark red solution, 2,2′-bipyridine (0.024 mg, 0.8 mmol) and NH_4PF_6 (0.26 g, 1.6 mmol) were added and dark violet microcrystalline material was filtered by suction. Dark violet tablets suitable for X-ray analysis were obtained by layering a solution of **1** in acetonitrile with chloroform. Elemental analysis calcd for $C_{84}H_{64}F_{24}Fe_4N_{20}P_4$: C 46.78, H 2.99, N 12.99; found: C 46.78, H 3.20, N 12.89.

$[Fe^{II}_2Co^{II}_2(\mu\text{-}CN)_4(bpy)_8](PF_6)_4\cdot 3CHCl_3\cdot 2CH_3CN$ (2): $[Fe^{II}(CN)_2(bpy)_2]$ (55 mg, 0.13 mmol) in MeOH (25 mL) was added to a solution of $CoCl_2\cdot 6H_2O$ (31 mg, 0.13 mmol) and bpy (41 mg, 0.26 mmol) in methanol (25 mL). After the mixture had been stirred for a day, addition of NH_4PF_6 (85 mg, 0.52 mmol) in methanol (25 mL) gave a red powder. Recrystallization by slow diffusion of chloroform into a solution of **2** in acetonitrile yielded red crystals. Elemental analysis calcd for $C_{84}H_{64}Co_2F_{24}Fe_2N_{20}P_4$: C 46.65, H 2.98, N 12.95; found: C 46.90, H 2.83, N 12.71.

$[Fe^{II}_2Co^{III}_2(\mu\text{-}CN)_4(bpy)_8](PF_6)_6\cdot 2CHCl_3\cdot 4CH_3NO_2$ (3): $[Fe^{III}(CN)_2(bpy)_2](PF_6)$[19] (61 mg, 0.13 mmol) in MeOH (25 mL) was added to a solution of $CoCl_2\cdot 6H_2O$ (31 mg, 0.13 mmol) in methanol (25 mL). After the mixture had been stirred for three days, addition of NH_4PF_6 (85 mg, 0.52 mmol) in methanol (25 mL) gave a brown powder. Recrystallization by slow diffusion of chloroform into a solution of **3** in nitromethane yielded dark red crystals. Elemental analysis calcd for $C_{84}H_{64}Co_2F_{36}Fe_2N_{20}P_6$: C 41.13, H 2.63, N 11.41; found: C 41.20, H 2.81, N 11.53.

Electrochemical measurements and UV/Vis spectra: Cyclic voltammetry (CV) and differential-pulse voltammetry (DPV) were carried out in nitrogen-purged acetonitrile solution at room temperature with use of a BAS CV-50W voltammetric analyzer. A glassy carbon electrode was used as the working electrode. The counter electrode was a platinum coil, and the reference electrode was a saturated sodium calomel electrode (SSCE). The concentration of the complexes was 1×10^{-3} M, and tetrabutylammonium hexafluorophosphate (0.1 M) was used as the suporting electrolyte. CV was performed at a scan rate of 100 mV s^{-1}. All the half-wave potentials $E_{1/2}=(E_{pc}+E_{pa})/2$, where E_{pc} and E_{pa} are the cathodic and anodic peak potential, respectively, are reported with respect to the SSCE in this study. Controlled-potential absorption spectra were obtained with an optically transparent thin-layer electrode (OTTLE) cell. The working electrode was platinum mesh. The counter electrode was a platinum coil. The reference electrode was an SSCE. Spectroelectrochemical measurements were carried out using a Hokutodenko HA-501 potentiostat. The OTTLE cell was cooled to about $-30\,^\circ$C. All electrochemical and spectroelectrochemical measurements were carried out under a nitrogen atmosphere.

Magnetic measurement: Magnetic susceptibility data were collected in the temperature range of 2.0 to 300 K and in an applied 10 K G field with the use of a Quantum Design model MPMS SQUID magnetometer. Pascal's constants[20] were used to determine the constituent atom diamagnetism.

Crystallography: Crystallographic data for **1**–**3** are listed in Table 4. The data were collected at $-70\,^\circ$C ($Mo_{K\alpha}=0.71073$ Å) on a Rigaku AFC7S diffractometer for **1** and **3** and on a Bruker SMART 1000 diffractometer fitted with a CCD-type area detector for **2** by using the ω-2θ scan method, within the limits $2<\theta<25^\circ$ (**1**), $2<\theta<26$ (**2**), and $2<\theta<25^\circ$ (**3**). An empirical absorption correction was applied (SADABS for **2**, and psi-scan for **1** and **2**). The structures were solved by direct methods and refined by the full-matrix least-squares method on all F^2 data by using SHELEX-97 (G. M. Sheldrick, Universität Göttingen, Germany, **1997**) for **1** and **3** and by using the SHELXTL 5.1 package (Bruker Analytical X-ray Systems) for **2**. All non-hydrogen atoms were refined with anisotropic thermal parameters. Hydrogen atoms were included in calculated positions and refined with isotropic thermal parameters riding on the parent atoms. One of the PF_6^- ions in **1**–**3** was found to be disordered and a split-atom model with a 1:1 occupancy was applied. Crystallographic data (excluding structure factors) for the structures reported in this paper have been deposited with the Cambridge Crystallographic Data Centre as supplementary publication no. CCDC-136744 (**1**), CCDC-136745 (**2**), and CCDC-136746 (**3**). Copies of the data can be obtained free of charge on application to CCDC, 12 Union Road, Cambridge CB2 1EZ, UK (fax: (+44) 1223-336-033; e-mail: deposit@ccdc.cam.ac.uk).

Table 4. Crystal data and structure refinement for **1**–**3**.

	1	**2**	**3**
chemical formula	$C_{84}H_{72}F_{24}Fe_4N_{20}O_4P_4$	$C_{91}H_{73}Cl_9Co_2F_{24}Fe_2N_{22}P_4$	$C_{90}H_{78}Cl_6Co_2F_{36}Fe_2N_{24}O_8P_6$
fw	2228.88	2603.24	2935.84
T [°C]	−100	−70	−70
crystal system	triclinic	triclinic	monoclinic
space group	$P\bar{1}$ (no.2)	$P\bar{1}$ (no.2)	$P2_1/n$ (no.14)
a [Å]	15.216(3)	13.501(3)	14.735(5)
b [Å]	24.108(3)	14.138(3)	15.429(4)
c [Å]	13.359(2)	29.243(6)	25.421(3)
α [°]	100.18(1)	77.43(3)	
β [°]	101.64(1)	81.04(3)	95.42(2)
γ [°]	74.46(1)	82.32(3)	
volume [Å^3]	4585(1)	5353.0(18)	5754(3)
Z	2	2	2
λ [Å]	0.71073	0.71073	0.71073
ρ_{calcd} [g cm^{-3}]	1.794	1.612	1.692
$\mu(Mo_{K\alpha})$ [mm^{-1}]	0.816	0.994	0.805
transmission coeff.	0.930–0.988	0.624–0.894	0.920–0.975
obs. refl. criterion	$I>2\sigma(I)$	$I>2\sigma(I)$	$I>2\sigma(I)$
$R1$[a]	0.0518	0.0691	0.0754
$R2$[b]	0.1456	0.1800	0.1837

[a] $R1=\Sigma||F_o|-|F_c||/\Sigma|F_o|$. [b] $wR2=[\Sigma[w(F_o^2-F_c^2)^2]/\Sigma[w(F_o^2)^2]]^{0.5}$, $w=1/[\sigma^2(F_o^2)+(0.1008P)^2+7.3710P]$ for **1**, $w=1/[\sigma^2(F_o^2)+(0.1258P)^2+2.6557P]$ for **2**, and $w=1/[\sigma^2(F_o^2)+(0.1126P)^2+7.4704P]$ for **3** where $P=(F_o^2+2F_c^2)/3$.

Acknowledgement

This work was partially supported by a Grant-in-Aid for Scientific Research from the Ministry of Education, Science, Sports and Culture, Japan.

[1] a) A. Ito, M. Suenaga, K. Ono, *J. Chem. Phys.* **1968**, *48*, 3597; b) T. Mallah, S. Thiebaut, M. Verdaguer, P. Veillet, *Science* **1993**, *262*, 1554; c) W. R. Entley, G. S. Girolami, *Science* **1995**, *268*, 397; d) V. Gadet, T. Mallah, I. Castro, P. Veillet, M. Verdaguer, *J. Am. Chem. Soc.* **1992**, *114*, 9213; e) W. D. Griebler, D. Babel, *Z. Naturforsch. B* **1982**, *87*, 832; f) S. Ferlay, T. Mallah, R. Quaès, P. Veillet, M. Verdaguer, *Inorg. Chem.* **1999**, *38*, 229; g) S. Ferlay, T. Mallah, R. Ouahès, P. Veillet, M. Verdaguer, *Nature* **1995**, *378*, 701; h) O. Sato, T. Iyoda, A. Fujishima, K. Hashimoto, *Nature* **1996**, *271*, 49; i) W. R. Entley, G. S. Girolami, *Inorg. Chem.* **1994**, *33*, 5165; j) J. Larionova, R. Clérac, J. Sanchiz, O. Kahn, S. Golhen, L. Ouahab, *J. Am. Chem. Soc.* **1998**, *120*, 13088.

[2] a) A. N. Holden, B. T. Matthias, P. W. Anderson, H. W. Lewis, *Phys. Rev.* **1956**, *102*, 1463; b) R. M. Bozorth, H. J. Williams, D. E. Walsh, *Phys. Rev.* **1956**, *103*, 572.

[3] a) O. Sato, T. Iyoda, A. Fujishima, K. Hashimoto, *Science* **1996**, *272*, 704; b) M. Verdaguer, *Science* **1996**, *272*, 698.

[4] a) D. G. Fu, J. Chen, X. S. Tan, L. J. Jiand, S. W. Zhang, P. J. Zheng, W. X. Tang, *Inorg. Chem.* **1997**, *36*, 220; b) K. V. Langenberg, S. R. Batten, K. J. Berry, D. C. R. Hockless, B. Moubaraki, K. S. Murray, *Inorg. Chem.* **1997**, *36*, 5005.

[5] a) A. Scuiller, T. Mallah, M. Verdaguer, A. Nivorozkhin, J-L. Tholence, P. Veillet, *New J. Chem*. **1996**, *20*, 1; b) T. Mallah, C. Auberger, M. Verdaguer, P. Veillet, *J. Chem. Soc. Chem. Commun*. **1995**, 61; c) N. Vernier, G. Bellessa, T. Mallah, M. Verdaguer, *Phys. Rev. B* **1997**, *56*, 75.
[6] a) J. L. Heinrich, P. A. Berseth, J. R. Long, *Chem. Commun*. **1998**, 1231; b) K. K. Klausmeyer, T. B. Rauchfuss, S. R. Wilson, *Angew. Chem*. **1998**, *110*, 1808; *Angew. Chem. Int. Ed*. **1998**, *37*, 1694.
[7] H. Vahrenkamp, A. Geiß, G. N. Richardson, *J. Chem. Soc. Dalton Trans.* **1997**, 3643.
[8] S. Zhan, Q. Meng, X. You, G. Wang, P. Zheng, *Polyhedron* **1996**, *15*, 2655.
[9] a) T. -H. Lu, H. -Y. Kao, D. I. Wu, K. C. Kong, C. H. Cheng, *Acta Crystallogr. Sect. C* **1988**, *44*, 1184; b) A. A. Schilt, *Inorg. Chem*. **1964**, *3*, 1323.
[10] The mononuclear compound $[Fe(CN)_2(bpy)_2]$ showed a reversible wave at 0.47 V vs. SSCE, which is much less positive than that for the square.
[11] a) V. Balzani, A Juris, M. Venturi, S. Campagna, S. Serroni, *Chem. Rev*. **1996**, *96*, 759; b) C. A. Bignozzi, J. R. Schoonover, F. Scandola, *Prog. Inorg. Chem*. **1997**, *44*, 1.
[12] C. A. Bignozzi, S. Roffia, C. Chiorboli, J. Davila, M. T. Indelli, F. Scandola, *Inorg. Chem*. **1989**, *28*, 4350.
[13] N. S. Hush, *Prog. Inorg. Chem*. **1967**, *8*, 391; C. Creutz, *Prog. Inorg. Chem*. **1983**, *30*, 1.
[14] R. Glauser, U. Hauser, F. Herren, A. Ludi, P. Roder, E. Schmidt, H. Siegenthaler, F. Wenk, *J. Am. Chem. Soc*. **1973**, *95*, 8458.
[15] C. A. Bignozzi, S. Roffia, C. Chiorboli, J. Davila, M. T. Indellim, F. Scandola, *Inorg. Chem.* **1989**, *28*, 4350.
[16] M. B. Robin, P. Day, *Adv. Inorg. Chem. Radiochem*. **1967**, *10*, 247.
[17] D. E. Richardson, H. Taube, *Inorg. Chem*. **1981**, *20*, 1278.
[18] A. A. Shilt, *Inorg. Synth*. **1970**, *Vol. XII*, 249.
[19] A. A. Shilt, *J. Am. Chem. Soc*. **1960**, *82*, 3000.
[20] W. E. Hatfield, *Theory and Application of Molecular Paramagnetism* (Eds.: E. A. Boudreaux, L. N. Mulay), Wiley, New York, **1976**, pp. 491 – 495.

Received: September 3, 1999 [F2018]

  0947-6539/00/0614-2530 $ 17.50+.50/0